Spectral Degeneracy Breaking of the Plasmon Resonance of Single Metal Nanoparticles by Nanoscale Near-Field Photopolymerization

H. Ibn El Ahrach, R. Bachelot,* A. Vial, G. Lérondel, J. Plain, and P. Royer

Laboratoire de Nanotechnologie et d'Instrumentation Optique, ICD CNRS FRE 2848, Université de Technologie de Troyes, 12 rue Marie Curie, BP 2060 10010 Troyes Cedex, France

O. Soppera

Département de Photochimie Générale, CNRS UMR 7525, Maison du Technopole, 34 rue Marc Seguin BP 72005, 68058 Mulhouse Cedex, France

(Received 8 September 2006; published 8 March 2007)

We report on controlled nanoscale photopolymerization triggered by enhanced near fields of silver nanoparticles excited close to their dipolar plasmon resonance. By anisotropic polymerization, symmetry of the refractive index of the surrounding medium was broken: $C\infty v$ symmetry turned to $C2v$ symmetry. This allowed for spectral degeneracy breaking in particles plasmon resonance whose apparent peak became continuously tunable with the incident polarization. From the spectral peak, we deduced the refractive-index ellipsoid fabricated around the particles. In addition to this control of optical properties of metal nanoparticles, this method opens new routes for nanoscale photochemistry and provides a new way of quantification of the magnitude of near fields of localized surface plasmons.

DOI: 10.1103/PhysRevLett.98.107402 PACS numbers: 78.67.Bf, 36.40.Gk, 82.35.Np

There has been recent considerable interest in resonant metal nanostructures (MNS) [1]. The most important optical phenomenon encountered in MNS is electromagnetic surface plasmon resonance (SPR) due to collective oscillations of the conduction electrons [1–4]. SPR is responsible for formerly and recently reported rich physical effects and phenomena such as MNS's apparent colors [5], local field enhancement [6], and photoluminescence [7]. Related challenges and applications are numerous. They include future integrated optics based on metals [8,9], high sensitivity nanosensors [10], surface enhanced Raman spectroscopy [11], nanophotolithography [12], and near-field optical microscopy and spectroscopy [13,14]. A lot of effort has thus been dedicated to the control of electron resonance in nanometals. To this purpose, using electron lithography [15] and chemical synthesis [16] a large variety of MNS shapes were obtained. Geometric anisotropies [17], nanoshells configuration [18], and control of distances between particles [19–22] lead to a wide range of possible plasmon resonances from the near UV to the near-IR. At the same time, a large effort was made to characterize the involved optical phenomena using near-field scanning optical microscopy [23].

In this Letter we present a new approach for both controlling and studying the optical properties of resonant metal nanoparticles. Our approach is based on controlled nanoscale photopolymerization triggered by local enhanced electromagnetic fields of the particles. Three main points are here emphasized. First, our approach opens the door to nanophotochemistry of polymers. Second, it constitutes a new way of quantifying the field enhancement associated with localized surface plasmon resonance. Third, it allows for control of the optical properties of the MNS: the spatially inhomogeneous electromagnetic intensity distribution enhanced by the underlying surface plasmon leads to an anisotropic polymerization around the particles, introducing thus a degree of SPR tunability. While further experiments are under way, the data presented in this Letter concern mainly the third point.

Silver was chosen to achieve mutual spectral overlapping between photopolymer absorption and SPR of the MNS embedded in liquid polymer. The silver nanoparticles were manufactured on a glass substrate by electron beam lithography. The sample consists of 500 nm period arrays of disk-shaped nanoparticles with a diameter of 70 nm and a height of 50 nm. A drop of liquid photopolymerizable formulation, described elsewhere [24], was deposited on the patterned substrate. Photopolymerization relies on production of free radicals and is characterized by a nonlinear threshold behavior allowing for high resolution patterning under evanescent illumination [24]. After formulation deposition, the sample was illuminated ($\lambda = 514$ nm) in normal incidence by a linearly polarized plane wave. The incident energy was below the threshold so that polymerization occurs only around MNS where local near fields are enhanced.

Knowledge of the threshold value ensures control of the procedure and is therefore of prime importance. This threshold was determined by using two beam interference pattern as a reference. Figure 1 gives insight into the nonlinear response of the polymer. Figure 1(a) shows atomic force microscopy (AFM) image of the polymer pattern obtained after a 20 mJ/cm^2 exposure. The exposure was followed by rinsing with methanol to remove any unpolymerized parts. The image shows that almost all the parts of the fringes participated to the polymerization, and the cyclic rate is 1 [see Fig. 1(c)]. Figure 1(b) shows an AFM image of the pattern obtained for a lower energy

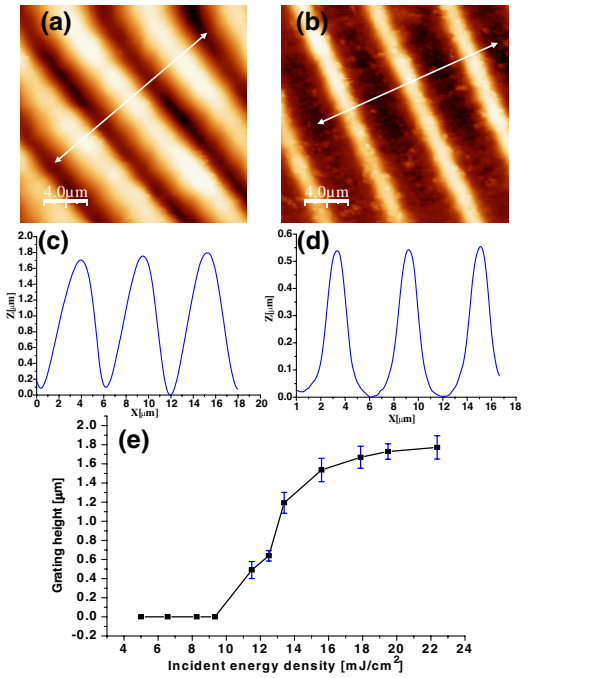

FIG. 1 (color online). Determination of the threshold energy. (a) and (b) AFM image of polymer grating obtained after 20 mJ/cm^2 and 11.5 mJ/cm^2 exposures, respectively. (c) and (d) corresponding profiles. (e) Grating height as a function of incident energy density.

density (11.5 mJ/cm^2). Here, only the peak of the fringes triggered polymerization, leading to an apparent cyclic rate to about 0:3 [see Fig. 1(d)]. Figure 1(e) shows the height of the polymer grating as a function of incident energy density. No grating was obtained for an incident energy density below 10 mJ/cm^2. This value was considered to be the threshold value.

This characterized formulation was used for near-field photochemical interaction with the MNS. The MNS covered by the formulation were illuminated with an incident energy density 4 times weaker than the threshold of polymerization. The sample was then rinsed, dried with nitrogen, and UV post-irradiated to complete and stabilize the polymerization. Figures 2(a) and 2(b) show the result of the experiment as imaged by AFM. Two symmetric polymer lobes built up close to the particles can be observed, resulting in metal-polymer hybrid particles. The two lobes originate from the excitation of MNS's dipolar SPR, as numerically illustrated in Fig. 2(c) obtained through a finite difference time domain (FDTD) calculation [25]. The field distribution associated with the resonance is enhanced in a two-lobe region oriented with the incident polarization. The localized nanoscale photopolymerization is the result of the inhomogeneous field distribution showed in Fig. 2(c). The two lobes can be viewed as a three-dimensional polymer molding of the locally enhanced optical fields. Figures 2(a) and 2(b) show that it is possible to control nanoscale photopolymerization in the visible region of the spectrum by using the near field of

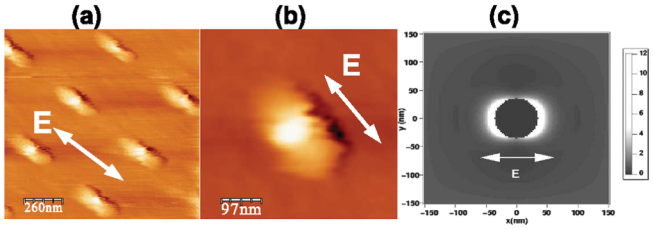

FIG. 2 (color). (a) and (b) AFM images recorded after irradiation and developing of the silver nanoparticles arrays covered with the photopolymerizable formulation. (c) Intensity distribution in the vicinity of an Ag particle embedded in the formulation as calculated by FDTD method ($\lambda = 514$ nm). The white arrow represent the incident polarization used for exposure.

resonant metal nanoparticles. This control was made possible by precise knowledge of the polymerization threshold and results from the abilities of the confined optical near field of MNS to quickly consume dissolved oxygen at the nanometer scale (oxygen acts as an inhibitor of polymerization [24]). Figure 2 also shows that the intrinsic resolution of the material is very high. The possibility to trigger photopolymerization at the nanoscale will enable local quantification of crucial photochemical parameters, including initiation of the polymerization, involved charges transfers, deexcitation of eosin triplet state, and peroxidation of the radicals [24].

On the other hand, our approach constitutes a unique way of quantifying the field enhancement associated with localized surface plasmon resonance. This quantification relies on the precise knowledge of a value characteristic of the photosensitive material: the threshold energy. In the present case, we learn that the intensity enhancement factor is greater than 4 because the polymerization threshold was locally exceeded. This result is in agreement with the calculated enhancement factor of 12 shown in Fig. 2(c). We performed the same exposure using gold particles instead of silver particles. No local polymerization was observed. This is certainly due to the fact that off-resonance enhancement factor is not superior to 4. This point was confirmed by FDTD calculation that predicted an intensity enhancement factor of about 3.5 for embedded gold particles at $\lambda = 514$ nm. Further studies based on multiple exposures and dichotomy will allow us to quantify precisely the enhancement factors involved in SPR.

Figure 2 shows that polymerization was not isotropic due to the inhomogeneous nature of the actinic field. This suggests that the modification of the Ag particle's plasmon resonance due to local change of the medium is not isotropic. This is confirmed by Fig. 3. The top of Fig. 3 shows extinction spectra of the array taken under different conditions. Spectrum (a) is the initial spectrum of the particles deposited on glass exposed in air. Spectrum (b) shows a 50 nm redshift in the liquid polymer (just before exposure). For spectra (a) and (b), the SPR has, within the sample plane, an isotropic response to the polarization due to the circular symmetry of the particles. Spectra of the hybrid

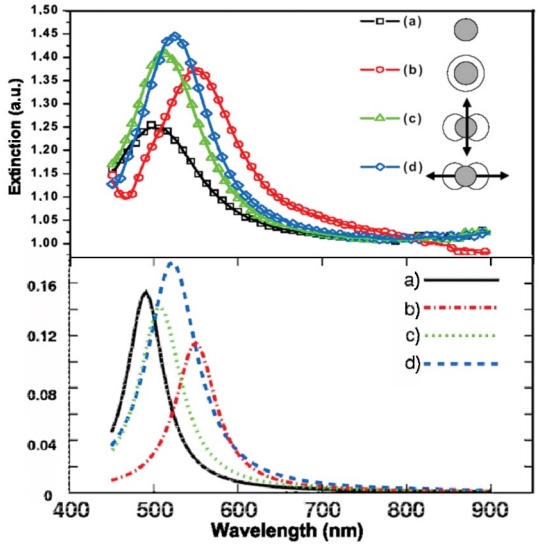

FIG. 3 (color). The extinction spectra from a silver nanoparticle array. Top: experimental data. (a) Array in air on a glass substrate. (b) Array in initial liquid polymer (before exposure). (c) on hybrid particles excited along the minor axis (d) on hybrid particles excited along the major axis. Bottom: corresponding theoretical spectra.

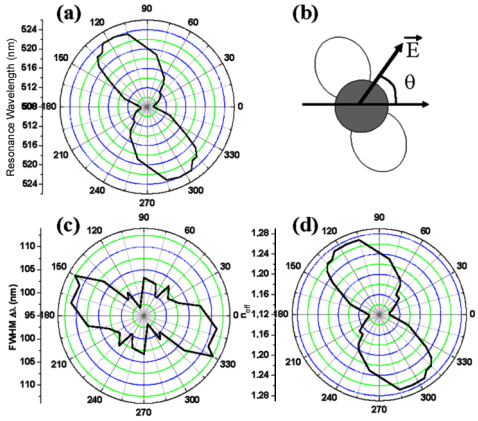

FIG. 4 (color online). Polar diagrams: data as a function of the polarization angle around the hybrid nanoparticles: (a) SPR peak; (b) experimental configuration; (c) spectral FWHM; (d) effective refraction index.

particles were measured for two extreme polarization angles. Spectrum (d) was measured for a polarization parallel to the major axis of the hybrid particle. Compared to spectrum (a), it shows a 28 nm redshift in the resonance. Spectrum (c) was obtained for a polarization perpendicular to the minor axis of the hybrid particle. Compared to spectrum (a), an 8 nm redshift is observed. The anisotropy of the medium surrounding the particle is the consequence of these two different redshifts and are the indicators of a spectral degeneracy breaking. This was confirmed by electromagnetic calculations shown on the bottom of Fig. 3. The graph shows FDTD spectra obtained for the four configurations depicted in the top of Fig. 3. A Drude model was used to describe the Silver dielectric constant [25]. The used parameters corresponded to the experimental condition. In particular, the substrate was included. Permeability at infinity, plasma frequency, damping coefficient, substrate index, and polymer index, were 4.0556, 8.8036 eV, 0.13117 eV, 1.508, and 1.52, respectively. The simulated spectra are in good agreement with experimental ones. In particular, along the major axis, the extinction amplitude rises with increasing the surrounding permittivity as the result of a change in the polarizability. Before local photopolymerization, metallic nanoparticles are characterized by a $C\infty v$ symmetry corresponding to the rotation Cv axis [26]. After polymerization, the two polymerized lobes induce a new lower symmetry: $C2v$, for which any pattern is reproduced by π in-plane rotation. This new symmetry induces the breakdown of the SPR spectral degeneracy. Figure 4(a) is a polar diagram of SPR peaks obtained by measuring 50 spectra of the hybrid particles for different angles of polarization θ as illustrated in Fig. 4(b). The two polymerized lobes clearly induced a quasicontinuously tunable SPR in the [508–522] nm range. The local polymerization leads to two plasmon eigenmodes centered at 508 and 522 nm, respectively. For any polarization angle θ, a linear combination of the two eigenmodes is excited, with respective weights depending on the polarization direction. We conclude that the apparent continuous plasmon tuning is the result of a shift in position of the barycenter of the spectral linear combination. This is confirmed by Fig. 4(c) showing a polar full width at half maximum (FWHM) of the spectra acquired in Fig. 4(a). The FWHM is maximum for a polarization at 45° relative to the axis of the hybrid particle, where both eigenmodes are equally excited. These results confirm the importance of symmetry in a nanoparticle in nanophotonics [27].

These data can be discussed in terms of nanoscale effective index distribution $n_{\text{eff}}(\theta)$. This function expresses the effect of the respective weights of the eigenmodes on an effective refractive index around MNS under a particular polarization direction defined by θ. n_{eff} is equal to $n_m + \Delta n_m$, where $n_m = \varepsilon_m^{1/2}$ is the initial refraction index of the external medium taken as a reference and Δn_m is the polymerization-induced shift in the refractive index. n_m was chosen to be 1.48 [24] (silver particles embedded in photopolymer formulation before exposure). By differentiating the denominator of the particule polarizability [28] and using published value of ε, the silver dielectric constant [29], Δn_m was deduced from $\Delta\lambda = -4n_m\Delta n_m(d\epsilon/d\lambda)^{-1}$, where $\Delta\lambda$ is the measured shift of SPR peak relative to the reference spectrum. The derivation was performed for spherical particles which is a good approximation for in-plane measurements. n_{eff} was deduced from the spectra of Fig. 4(a). For Ag particles in air deposited on a glass substrate, n_{eff} is found to be 1.06 as a result of the modification of the SPR by the glass-air interface. For the hybrid particles the θ dependence of the surrounding effective index is shown in Fig. 4(d). An

effective index of ~1.15 is found for an excitation along the minor axis (suggesting the presence of thin polymer layer along this axis) while the major axis is associated to a ~1.3 index, as a consequence of a thicker polymer region along this axis. Note that the bulk polymer index is 1.52 [24]. The difference between the effective index associated with the long axis and the bulk value can be attributed to the spatial extent of polymerization which is limited by the threshold value. The field surrounding the hybrid particle extends beyond the area defined by the two polymerized lobes resulting in a lower effective index. Between the two extreme values, a continuous $n_{\mathrm{eff}}(\theta)$ is observed.

In conclusion, we demonstrated controlled nanoscale photopolymerization in the near field of resonant metal nanoparticles. This approach opens new routes for nanophotochemistry and offers a unique way of quantifying field enhancement factors in localized surface plasmons. Additionally, it allows for control of optical properties of MNS. More precisely in this Letter, by anisotropic nanoscale photopolymerization we demonstrated a controlled breaking of symmetry governing the dielectric environment of silver nanoparticles. Starting from an original $C\infty v$ symmetry, two artificial plasmon eigenmodes are created as a result of a new $C2v$ symmetry. An inhomogeneous distribution of effective refractive index around the spherical particle was deduced and is responsible for a spectral degeneracy breaking of the surface plasmon resonance. The method allowed thus the controlled production of a dielectric encapsulant that can be viewed as an artificial nanometric refractive-index ellipsoid. The approach presented here has unique and numerous advantages compared to the standard approaches based on control of the geometry of the metal particles. In particular, several properties and processes involved in polymer science [30] can be coupled to (or assisted by) MNS at the nanoscale. They include nonlinear or electro-optical properties, possible doping with luminescent (non) organic materials and chemical control of the refractive index. Furthermore, different degrees of symmetry could be achieved by using high order plasmon modes selected by proper incident polarization or wavelength. We believe this approach is an important first step toward a new and efficient control of optical behavior of metal nanostructures.

The authors thank A. Bouhelier, J. J. Greffet, R. Carminati, and P. M. Adam for fruitful discussions and the region Champagne Ardenne for funding.

*To whom all correspondence should be addressed.
Email address: renaud.bachelot@utt.fr

[1] U. Kreibig and M. Vollmer, *Optical Properties of Metal Clusters* (Springer, Berlin, 1995).
[2] E. Hutter and J. H. Fendler, Adv. Mater. **16**, 1685 (2004).
[3] T. Klar, M. Perner, S. Grosse, G. von Plessen, W. Spirkl, and J. Feldmann, Phys. Rev. Lett. **80**, 4249 (1998).
[4] A. V. Zayats and I. Smolyaninov, J. Opt. A Pure Appl. Opt. **5**, S16 (2003).
[5] M. Faraday, Phil. Trans. R. Soc. London **147**, 145 (1857).
[6] N. Calander and M. Willander, Appl. Phys. Lett. **92**, 4878 (2002).
[7] A. Bouhelier, R. Bachelot, G. Lerondel, S. Kostcheev, P. Royer, and G. P. Wiederrecht, Phys. Rev. Lett. **95**, 267405 (2005).
[8] M. L. Brongersma, J. W. Hartman, and H. A. Atwater, Phys. Rev. B **62**, R16356 (2000).
[9] A.-L. Baudrion, J.-C. Weeber, A. Dereux, G. Lecamp, P. Lalanne, and S. I. Bozhevolnyi, Phys. Rev. B **74**, 125406 (2006).
[10] A. J. Haes and R. P. V. Duyne, Anal. Bioanal. Chem. **379**, 920 (2004).
[11] G. Laurent, N. Felidj, J. Aubard, G. Levi, J. Krenn, A. Hohenau, G. Schider, A. Leitner, and F. Aussenegg., J. Chem. Phys. **122**, 011102 (2005).
[12] C. Hubert, A. Rumyantseva, G. Lerondel, J. Grand, S. Kostcheev, L. Billot, A. Vial, R. Bachelot, P. Royer, S.-h. Chang, S. K. Gray, G. P. Wiederrecht, and G. C. Schatz, Nano Lett. **5**, 615 (2005).
[13] T. Kalkbrenner, U. Hakanson, A. Schadle, S. Burger, C. Henkel, and V. Sandoghdar, Phys. Rev. Lett. **95**, 200801 (2005).
[14] N. Anderson, P. Anger, A. Hartschuh, and L. Novotny, Nano Lett. **6**, 744 (2006).
[15] B. Lamprecht, G. Schider, R. T. Lechner, H. Ditlbacher, J. R. Krenn, A. Leitner, and F. R. Aussenegg, Phys. Rev. Lett. **84**, 4721 (2000).
[16] N. R. Jana, L. Gearheart, and C. J. Murphy, Adv. Mater. **13**, 1389 (2001).
[17] K. L. Kelly, E. Corondo, L. L. Zhao, and G. C. Schatz, J. Phys. Chem. B **107**, 668 (2003).
[18] R. D. Averitt, D. Sarkar, and N. J. Halas, Phys. Rev. Lett. **78**, 4217 (1997).
[19] A. Bouhelier, R. Bachelot, J. S. Im, G. P. Wiederrecht, G. Lerondel, S. Kostcheev, and P. Royer, J. Phys. Chem. B **109**, 3195 (2005).
[20] K.-H. Su, Q.-H. Wei, X. Zhang, J. J. Mock, D. R. Smith, and S. Schultz, Nano Lett. **3**, 1087 (2003).
[21] P. Ghenuche, R. Quidant, and G. Badenes, Opt. Lett. **30**, 1882 (2005).
[22] P. Nordlander, C. Oubre, E. Prodan, K. Li, and M. I. Stockman, Nano Lett. **4**, 899 (2004).
[23] G. P. Wiederrecht, Eur. Phys. J. Appl. Phys. **28**, 3 (2004).
[24] A. Espanet, G. D. Santos, C. Ecoffet, and D. J. Lougnot, Appl. Surf. Sci. **138**, 87 (1999).
[25] A. Vial, A.-S. Grimault, D. Maćıas, D. Barchiesi, and M. Lamy de la Chapelle, Phys. Rev. B **71**, 085416 (2005).
[26] H. Tinkham, *Group Theory and Quantum Mechanics* (McGraw-Hill, New York, 1964).
[27] H. Wang, Y. Wu, B. Lassiter, C. L. Nehl, J. H. Hafner, P. Nordlander, and N. J. Halas, Proc. Natl. Acad. Sci. U.S.A. **103**, 10856 (2006).
[28] C. F. Bohren and D. R. Huffman, *Absorption and Scattering of Light by Small Particles* (John Wiley & Sons, Inc., New York, 1998).
[29] E. D. Palik, *Handbook of Optical Constants of Solids* (Academic Press, Orlando, FL, 1985).
[30] *Physical Properties of Polymers Handbook*, edited by J. E. Mark (Springer-Verlag, New York, 2007), 2nd ed.